STEADY STALL AND COMPRESSIBILITY EFFECTS ON HINGELESS ROTOR AEROELASTICITY IN HIGH-G TURNS

Roberto Celi*
Department of Aerospace Engineering
University of Maryland, College Park, USA

Abstract

This paper describes a numerical study of the aeroelastic stability of a hingeless rotor helicopter in a steady coordinated turn. A quasi-steady aerodynamic model is used, which includes airfoil stall and compressibility effects. The finite element model of the rotor blades includes kinematic nonlinearities due to moderately large elastic deflections. The results show that the lag modes are stabilized in level turns. In descending flight, the first lag mode is unstable at low turn rates, and the damping of the second lag mode decreases sharply at medium turn rates. Strong aerodynamic nonlinearities introduce multiple trim solutions and make the predicted stability levels very sensitive to changes in pitch control settings.

Nomenclature

a	Lift curve slope
b	Blade semichord
c_d	Airfoil drag coefficient
c_m	Airfoil pitching moment coefficient
c_n	Airfoil normal force coefficient
f	Chordwise position of the separation point, as a fraction of the blade chord
g	Acceleration due to gravity
k	Goldstein's circulation correction factor
n_T	Load factor
R	Main rotor radius
V	Flight speed of the helicopter
v, w	Blade elastic deformation in lag and flap
x	Blade spanwise coordinate, as a fraction of the rotor radius
$\bar{x}_A$	Chordwise offset of aerodynamic center from the elastic axis divided by blade semichord, positive for a.c. ahead of e.a.
β	Sideslip angle
γ	Flight path angle, positive for climbing flight
ζ	Real part of characteristic exponent
θ_G	Total geometric blade pitch angle
θ_0	Blade collective pitch angle
μ	Advance ratio
ρ_A	Air density
ϕ	Torsional elastic deformation of the blade
ψ	Blade azimuth angle
$\dot{\psi}$	Aircraft turn rate, positive for right turns
Ω	Rotor angular velocity

Subscripts

$(\,)_{,x}$	$\dfrac{\partial}{\partial x}$

Introduction and Problem Statement

Steep turns represent important flight conditions for military and civil helicopters alike. They may be required to seek cover and avoid detection, to engage or escape from enemy threats, or to prevent collisions with suddenly appearing obstacles or other aircraft. Substantial rotor loads develop in these flight conditions, together with relatively high roll, pitch, and yaw rates. Large portions of the rotor disk are stalled or near stall.

Limited information on the effects of steep turns on the aeroelastic stability of a helicopter rotor exists in the published literature, as shown by recent comprehensive survey papers [1,2]. With the exception of flight in turbulent atmosphere, most research work on rotary-wing aeroelasticity has focused on steady, straight, 1-g flight conditions. A series of detailed studies of the trim conditions and the flight dynamics of several rotorcraft types, including hingeless rotor helicopters, in steep, high-g turns has been conducted by Chen [3]-[5]. Although the mathematical model of the rotor was relatively simple because the focus was on flight mechanics, rather than aeroelasticity, these studies are particularly valuable because they define a complete set of exact kinematic relations for a helicopter in a steady, coordinated, helical turn.

In Ref. [6], a set of equations for trim based on those of Refs. [3] and [4] was coupled with an aeroelastic model of hingeless rotor blades undergoing moderate elastic deflections in coupled flap-lag-torsional motion. The resulting mathematical model was used to investigate the trim state and the aeroelastic stability of a hingeless rotor helicopter in steady turning flight conditions. The effect of several turn parameters such as advance ratio, turn rate, flight path angle, and turn direction was studied. In Ref. [6] a very simple aerodynamic model was used in the analysis: stall, compressibility, and three-dimensional (3D) tip effects were neglected. In the study described in this paper, a number of improvements to the aerodynamic model are implemented, namely the modeling of quasi-steady stall and Mach number effects on the lift, drag, and pitching moment characteristics of the airfoil, and the introduction of simple corrections for 3D tip effects.

The main objective of this paper is to study the effects of airfoil stall and compressibility on the trim

*Assistant Professor, Center for Rotorcraft Education and Research

state and the aeroelastic stability of a trimmed hingeless rotor in a steady, coordinated turn. Of particular interest are the degradations in stability observed in Ref. [6] for the first lag mode in straight, descending flight, for the second lag mode in tight, descending left turns, and for some of the flap modes in tight, level turns. The effects of modeling assumptions are studied systematically by obtaining results with mathematical models of increasing complexity, in which the effects of angle of attack and Mach number are added one at the time.

Another objective of this paper is to observe the effects of increasing the nonlinearity of the overall aeroelastic rotor model. When linear incompressible aerodynamics is used, the nonlinearities in the mathematical model are due to the kinematics of moderate elastic deflections. These nonlinearities are relatively weak. On the other hand, the modeling of airfoil stall may introduce much stronger nonlinearities, which can increase the sensitivity of the aeroelastic stability levels to changes or inaccuracies in the equilibrium position about which the equations of motion are linearized.

Mathematical model

Coupled Trim and Aeroelastic Analysis

The aeroelastic analysis and the coupled trim procedure used to obtain the results of this paper are described in detail in Ref. [6], and only a brief outline is provided here.

The rotor blades are modeled as Bernoulli-Euler beams undergoing coupled flap-lag-torsional motion. The nonlinear, partial differential equations of motion of the blade are discretized using a finite element formulation based on Galerkin method of weighted residuals. The blades are attached to a hub of infinite mass, that is moving with prescribed angular velocities in pitch, roll, and yaw. The values of these velocities are provided by the solution of the coordinated turn trim problem, and are maintained fixed in the aeroelastic stability analysis.

The helicopter is assumed to be executing a steady, coordinated, helical turn. The coupled trim problem consists of the simultaneous solution of two sets of nonlinear algebraic equations.

The first set describes the trim state of the entire helicopter, and is based on the trim equations derived by Chen [3]. The set is composed of 13 equations: six enforcing force and moment equilibrium along and about the aircraft body axes, three relationships between roll, pitch and yaw rates and the Euler rates, two momentum theory equations for main and tail rotor inflow, and two additional kinematic relationships. The 13 unknowns are the collective pitch of the main rotor θ_0 and of the tail rotor θ_t, the longitudinal and lateral cyclic pitch settings θ_{1s} and θ_{1c}, the steady state roll, pitch, and yaw rates p, q, and r, the pitch attitude angle θ, the roll attitude angle ϕ, the aerodynamic angle of attack of the fuselage α, the sideslip angle β, and the constant portion of the inflow for the main rotor λ and the tail rotor λ_t. The turn rate $\dot{\psi}$ (> 0 for a right turn), the magnitude V of the aircraft velocity vector, and the flight path angle γ (> 0 for an ascending turn) define the turning flight condition, and are provided as input.

The second set of equations represents the blade aeroelastic response problem, which is coupled to the aircraft trim problem because the rotor forces and moments acting on the aircraft depend on the elastic deflections of the blades. The nonlinear ordinary differential equations (ODE) of motion of the blade are transformed into a set of nonlinear algebraic equations through a modal coordinate transformation followed by the application of a classical Galerkin method around the azimuth. The modal coefficients of the m modes used in the coordinate transformation are time (or azimuth) dependent, and are expanded in Taylor series truncated at the n-th harmonic. The $(2n+1)m$ Fourier coefficients are the unknowns of this portion of the trim problem. For all the results presented in this paper it is $m = 4$ and $n = 2$ for a total of 20 unknowns.

The system of nonlinear ODE that defines the aeroelastic stability and response problem is solved iteratively using quasilinearization. The solution of the set of ODE yields the steady-state, periodic equilibrium position of the rotor blades. The linearized stability of the system is evaluated, according to Floquet theory, by calculating the characteristic exponents of the state transition matrix at the end of one period, or rotor revolution. The small perturbation motion of the blade is stable if all the real parts of the characteristic exponent are negative. The required transition matrix is generated as part of the quasilinearization solution process.

Aerodynamic model

The aerodynamic loads acting on the rotor blades are treated using the implicit formulation extensively described in Ref. [7]. The expressions for the velocity components of the airflow at the cross-sections of an elastic blade undergoing coupled flap-lag-torsional motion, and attached to a moving hub, are presented in Ref. [8]. The incorporation of the effects of angle of attack α and Mach number M in the aerodynamic operator of the equations of motion is presented below.

The coordinate systems used in this study are the same as those of Ref. [9], and are shown in Figure 1. The $\hat{e}_x, \hat{e}_y, \hat{e}_z$ system is the undeformed blade coordinate system. The equations of motion of the blade are written in this coordinate system. The $\hat{e}'_x, \hat{e}'_y, \hat{e}'_z$ system is the deformed blade coordinate system. A rotation about the $\hat{e}'_x$ axis of an angle equal to the torsional deformation ϕ transform this coordinate system into the "double primed" coordinate system of unit vectors $\hat{e}''_x, \hat{e}''_y, \hat{e}''_z$.

The aerodynamic lift and moment per unit span can then be written in the following way:

$$L = a\rho_A U''_y bR\left[U''_y(\theta_G+\phi) - U''_z - (1.5-\bar{x}_A)bR\left(\dot{\theta}_G+\dot{\phi}\right)\Omega\right] \quad (1)$$

$$M = a\rho_A U''_y (bR)^2\left\{\bar{x}_A\left[U''_y(\theta_G+\phi) - U''_z\right] + (0.5-\bar{x}_A)bR\left(\dot{\theta}_G+\dot{\phi}\right)\Omega + 2\frac{k_{tip}c_m}{a}U''_y\right\} \quad (2)$$

and:

$$p''_{zA} = L\cos\left[\tan^{-1}\left(\frac{U''_z}{U''_y}\right)\right] \approx L \quad (3)$$

$$p''_{zA} = -L\sin\left[\tan^{-1}\left(\frac{U''_z}{U''_y}\right)\right] - \rho_A b R c_{d1}\left[\left(U''_y\right)^2 + \left(U''_z\right)^2\right]$$

$$\approx -\frac{U''_z}{U''_y}L - \rho_A b R c_{d1}\left[\left(U''_y\right)^2 + \left(U''_z\right)^2\right] \quad (4)$$

$$q''_{xA} = M \quad (5)$$

$$(6)$$

The aerodynamic loads in the undeformed coordinate system of unit vectors $\hat{e}_x, \hat{e}_y, \hat{e}_z$, are given by [9]:

$$p_{yA} = p''_{yA} - v_{,x}\, w_{,x}\, p''_{zA} \quad (7)$$

$$p_{zA} = p''_{zA} \quad (8)$$

$$q_{xA} = q''_{xA} \quad (9)$$

The lift curve slope a and the drag coefficient c_{d1} are given by:

$$a(x,\psi) = \frac{k c_n \cos\alpha - c_d \sin\alpha}{\alpha} \quad (10)$$

$$c_{d1}(x,\psi) = k c_n \sin\alpha + c_d \cos\alpha \quad (11)$$

with $\alpha = \theta_G + \phi$. The normal force coefficient c_n, the pitching moment coefficient c_m, and the drag coefficient c_d are calculated at each blade radial station x and azimuth angle ψ using the following equations due to Beddoes [10]:

$$c_n = c_{L\alpha}\alpha\left(\frac{1}{2} + \frac{1}{2}\sqrt{f}\right)^2 \quad (12)$$

$$c_m = c_n\left(k_0 + k_1 f + k_2 f^4\right) \quad (13)$$

$$c_d = c_{d0} + 0.035 c_n \sin\alpha + K_D c_n \sin\left(\alpha - \alpha_{DD}\right) \quad (14)$$

where f is the chordwise position of the separation point, given by:

$$f = \begin{cases} 1 - 0.3\exp\left(\dfrac{\alpha - \alpha_1}{S_1}\right) & \alpha < \alpha_1 \\ 0.66\exp\left(\dfrac{\alpha_1 - \alpha}{S_2}\right) + 0.04 & \alpha \geq \alpha_1 \end{cases} \quad (15)$$

and

$$K_D = \begin{cases} 0 & \alpha < \alpha_{DD} \\ 2.7\mathrm{e}^{-d_f f} & \alpha \geq \alpha_{DD} \end{cases} \quad (16)$$

The values of the parameters $c_{L\alpha}, \alpha_1, S_1, S_2, k_0, k_1, k_2, c_{d0}, \alpha_{DD}$, and d_f are provided in tabular form in Ref. [10], as a function of the Mach number M, for values of M ranging from 0.3 to 0.8. Curves of c_n, c_m, and c_d for the NACA 0012 airfoil are presented in Figures 2, 3, and 4 respectively, as a function of angle of attack α, for several values of the Mach number M. Throughout this study, the coefficients corresponding to $M = 0.3$ and $M = 0.8$ were used for all the values of $M \leq 0.3$ and $M \geq 0.8$ respectively. The effects of α and M are taken into account in both the coupled trim calculations and the aeroelastic stability and response calculations. For example, in the solution of the aeroelastic stability and response problem, the derivative of the aerodynamic load vector $\mathbf{A}$ with respect to the vector of generalized coordinates $\mathbf{y}$ is required. This derivative is a matrix, the i-th column of which is given, at the generic blade azimuth angle $\psi = \psi_0$, and at the k-th iteration of quasilinearization, by [7]:

$$\left[\frac{\partial \mathbf{A}}{\partial y_i}\right]^k_{\psi=\psi_0} \approx \frac{1}{h}\left\{\mathbf{A}\left[\mathbf{y}^k(\psi_0) + \mathbf{h}; \psi_0\right] - \mathbf{A}\left[\mathbf{y}^k(\psi_0); \psi_0\right]\right\} \quad (17)$$

where $\mathbf{h}$ is a vector with all its components equal to zero, except for the i-th, which is equal to a small number h. The matrix is square, and has size equal to the number of modes used in the modal coordinate transformation. In Eq. (17), the first and the second term inside square brackets are the aerodynamic load vectors corresponding to the perturbed and to the equilibrium motion of the blade respectively. Therefore these vectors are calculated with the values of c_l, c_d, and c_m corresponding to the appropriate blade distributions of α and M, that is, those associated with the perturbed and the equilibrium motion respectively.

Because the stall model is quasi-steady, certain aspects of the aeroelastic behavior of the blade that are associated with dynamic stall cannot be described accurately by the mathematical model used in this study. One such phenomenon is retreating blade stall flutter. The model, however, should be capable of capturing low frequency, stall-induced lag instabilities such as those predicted analytically and observed experimentally by Ormiston and Bousman [11].

The three-dimensional tip effects were taken into account approximately, by using Goldstein's circulation correction factor k_{tip} [12]

$$k_{tip} = \frac{2}{\pi}\cos^{-1}\mathrm{e}^{-f_G} \qquad f_G = \frac{b}{2}\frac{1-x}{x\sin\phi} \quad (18)$$

where ϕ is the inflow angle defined by:

$$\phi = \left|\tan^{-1}\frac{U''_z}{U''_y}\right| \quad (19)$$

Finally, Drees wake model was used to describe approximately the nonuniform inflow distribution over the rotor disk [13]:

$$\lambda = \lambda_0\left(1 + \kappa_x x\cos\psi + \kappa_y x\sin\psi\right) \quad (20)$$

with:

$$\kappa_x = \frac{4}{3}\left[\left(1 - 1.8\mu^2\right)\sqrt{1 + \left(\frac{\lambda}{\mu}\right)^2} - \frac{\lambda}{\mu}\right]$$

$$\kappa_y = -2\mu$$

Results

The blade configuration analyzed in this study is a uniform hingeless soft-in-plane blade configuration, with fundamental, rotating, coupled natural frequencies of 0.73/rev, 1.12/rev, and 3.17 /rev in lag, flap, and torsion respectively. The elastic coupling factor is $R = 1$, that is the elastic deformation of the blade occurs entirely outboard of the pitch bearing. The weight coefficient of the helicopter is $C_W = 0.005$. The solidity is $\sigma = 0.07$. Blade droop, sweep, precone, built-in twist, and chordwise offsets of aerodynamic centers and centers of mass from the elastic axis are equal to zero. The rotor blade chord is $c = 0.055R$, and the Lock number is $\gamma_L = 5.5$. The angular velocity of the rotor is $\Omega = 340$ RPM. The center of mass of the aircraft is placed at a distance of $0.02R$ in front of the mast, and $0.25R$ below the rotor head. The advance ratio is $\mu = 0.2$ for all the results presented in this paper.

The aeroelastic stability calculations were conducted using six coupled modes. In all cases these modes were the first three flap, the first two lag, and the first torsion coupled modes. Each generalized coordinate was represented as a five harmonic Fourier series. The initial approximation to the blade response, for the quasilinearization iteration, was generated using the same procedure as in Ref. [6]. For a given value of the advance ratio μ, the aeroelastic stability and response problem was solved for increasing values of the turn rate $\dot{\psi}$. The solution for a given value of the turn rate was used as the initial approximation for the next value of $\dot{\psi}$; the initial approximation for the straight flight cases, ($\dot{\psi} = 0$) was a rigid blade. Two iterations of quasilinearization were sufficient for most flight conditions below a turn rate of $\dot{\psi} = 0.25$ rad/sec. For higher values of the turn rate up to five iterations were required. Each iteration required 180-200 seconds of CPU time on an IBM 3081D computer for the cases in which the Mach number effects were not included in the model, and 240-320 seconds for the complete aerodynamic model.

In all the results presented in this paper, the curves marked "linear" show the results obtained using a linear incompressible aerodynamic model. In this case the lift curve slope, the pitching moment coefficient, and the drag coefficient of the airfoil were those corresponding to $\alpha = M = 0$ regardless of the actual local values of angle of attack and Mach number. In comparing the results with those of Ref. [6] it should be remembered that in the latter the linear model was based on a Glauert, rather than a Drees, inflow model, and 3D tip effects were neglected. For the curves marked "α effects only", the true angle of attack was used to calculate the airfoil coefficients, but the Mach number was arbitrarily set to zero. Thus c_l, c_d, and c_m were calculated using the curves for $M = 0.3$ in Figures 2, 3, and 4, regardless of the actual local value of M. These curves correspond to a nonlinear incompressible aerodynamic model. Finally, for the curves marked "α, M effects" both the true local values of α and of M were used. Thus these curves refer to a nonlinear compressible aerodynamics model. The curves referring to the nonlinear models are plotted for the entire range of values of the turn rate $\dot{\psi}$ for which it was possible to find a converged solution of the coupled trim problem. Because no limitations were posed on the available engine power, the coupled trim calculations performed using the linear incompressible aerodynamic model converged for much higher turn rates than shown in the plots.

The load factor n_T (defined according to Ref. [3]) is plotted in Figure 5, as a function of turn rate, for flight path angles of $\gamma = 0°$ and $\gamma = \pm 20°$. The results presented in this paper are obtained for turn rates of up to $\dot{\psi} = 25$ deg/sec, corresponding to a load factor of about 2.

Trim and aeroelastic stability in level turns

Figure 6 shows the values of collective pitch θ_0 required to sustain a steady coordinated turn, as a function of the turn rate. As expected, the most noticeable consequence of introducing nonlinear airfoil aerodynamics is a considerable reduction of the maximum possible turn rate. If the effects of Mach number are neglected, the trim values of collective pitch are essentially unaffected by the nonlinear airfoil aerodynamics. This mathematical model thus indicates that, as significant stall regions begin to appear on the rotor disk, a steady coordinated turn can no longer be maintained. When Mach number effects are included in the model, the trim value of the collective pitch increases sharply for turn rates greater than 15 deg/sec. This increase can be explained by observing the distribution of pitching moment coefficient over the rotor disk. In straight flight, the prevalent flow conditions encountered by the blade are such that the airfoils mostly operate at Mach numbers less than about 0.6 and angles of attack below 10 degrees. For this range of M and α the pitching moment coefficient c_m is positive, as indicated in Figure 3. Figure 7 confirms that over most of the rotor disk c_m is positive for this level flight condition. Therefore nose-up torsional deformations of the blade occur, and this reduces the value of θ_0 required for trim. As the turn rate increases, stall regions appear on the front of the rotor, and in portions of the third quadrant, as shown in Figure 8. In these regions, the value of c_m decreases, and nose-down pitching moments develop over small areas of the disk. The development of stall areas may explain the substantial increase of θ_0 for turn rates greater than 12-13 deg/sec shown in Figure 6.

Figure 9 shows the values of longitudinal and lateral cyclic pitch required to maintain the turn. The longitudinal cyclic θ_{1s} is largely unaffected by stall and compressibility for the range of turn rates for which a coordinated steady turn is possible. The linear and the nonlinear incompressible model produce essentially the same results for the lateral cyclic pitch θ_{1c}. However, when Mach number effects are included, substantially larger values of θ_{1c}, or more "left stick", are required.

Figure 10 shows the real part of the characteristic exponent of the first lag mode as a function of turn rate, for a level, right-handed turn. The figure shows that the results obtained with a linear and a nonlinear incompressible model are quite close. The small influence that stall has on the stability of the first lag mode is due to the fact that most of the rotor is oper-

ating below stall for all the flight conditions covered by the figure. On the other hand, the inclusion of Mach number effects increases considerably the stability of this mode. This stabilizing effect can be related to the fact that, over most of the rotor disk, the blade experiences nose-up pitching moments. Thus the effect of Mach number is to make the blade behave qualitatively like a blade with zero pitching moment coefficient, but with the aerodynamic center placed ahead of the elastic axis, $\bar{x}_A > 0$. The aeroelastic stability of blades with noncoincident elastic axis and aerodynamic centers has been studied in Ref. [7], where it was observed that positive values of $\bar{x}_A$ increase the damping of the first lag mode. This argument is also consistent with the large increase in damping that occurs with increasing turn rate. In fact, by comparing Figures 7 and 8 it can be seen that, as the turn rate increases, the portion of the disk over which c_m is positive decreases only slightly. On the other hand, the magnitude of the nose-up pitching moments increases considerably. Therefore, as the turn rate increases, the behavior of the blade becomes qualitatively similar to that of a blade with increasing, positive chordwise offset between aerodynamic center and elastic axis. The increasing positive offset increases the stability of the first lag mode.

The stability of the first torsion mode increases slightly when stall and compressibility effects are taken into account, as indicated by Figure 11. At high turn rates, however, the damping decreases considerably when a nonlinear compressible model is used. The nose-up pitching moments may be responsible for this destabilization, which is qualitatively similar to that caused by $\bar{x}_A > 0$, and observed in Ref. [7]. Finally, the real parts of the characteristic exponents for the first three flap modes are grouped in Figure 12. The behavior of the three modes with increasing turn rate is qualitatively similar. The damping remains essentially unchanged when a linear incompressible aerodynamic model is used. When angle of attack effects are included, the stability of these modes decreases at turn rates above 15-17 deg/sec. When the full nonlinear compressible aerodynamic model is used, the damping of the first and third lag modes starts decreasing at much lower turn rates, and the loss of damping is greater. However, these modes are highly damped and remain stable for the complete range of turn rates considered.

Trim and aeroelastic stability in descending left turns

Results were obtained for a descending flight condition, with $\gamma = -20°$. The turns were to the left, $\dot{\psi} < 0$, or counterclockwise as viewed from above. The reason for focusing on descending left turns is that in Ref. [6] it was found that the stability of the second lag mode decreases substantially in a descending turn, with a left turn being slightly more destabilizing than a right turn. Based on the criteria of Refs. [14] and [15], the descending flight conditions considered in this study are not expected to result in a vortex-ring state, therefore the use of momentum theory in the calculation of rotor inflow is legitimate.

Figures 13, 14, and 15, show respectively the trim values of sideslip angle β, collective pitch θ_0, and lateral cyclic pitch θ_{1c} as a function of the turn rate. These figures show that, when nonlinear airfoil characteristics are used, the solution of the coupled trim problem is not unique. For turn rates between 15 and 20 degrees per second approximately, at least one additional trim state can be defined. In particular, Figure 13 indicates that this additional trim state corresponds to a flight condition in which the helicopter exhibits large angles of sideslip with the nose pointing to starboard, that is away from the turn. The "basic" trim condition, on the other hand, corresponds to a relatively small sideslip angle, with the nose pointing slightly into the turn at low turn rates, and slightly away from the turn at higher turn rates. The predicted values of β are essentially insensitive to the modeling assumption, except at the highest turn rates. Figure 14 indicates that the values of θ_0 predicted using linear and nonlinear incompressible aerodynamics are almost identical. When Mach number effects are also taken into account, the large regions of nose-up pitching moments that appear over the rotor disk cause the collective pitch required for trim to decrease by about one degree for most values of turn rate. Much higher values of collective pitch are required for the high sideslip additional trim condition. The lateral cyclic pitch θ_{1c} is largely insensitive to the aerodynamic modeling assumptions, as shown in Figure 15, except for the highest values of turn rates where the nonlinear compressible model predicts about one more degree of left stick than the simpler models. Large values of left stick are required to sustain the high sideslip turn. In fact high values of β generates large aerodynamic side forces on the fuselage, directed away from the center of the turn, which must be balanced through large positive values of θ_{1c} coupled with the substantially increased values of collective pitch mentioned earlier. Based on a limited amount of numerical experimentation, it appears that no multiple solutions appear when a linear aerodynamic model is used, and that no more than two solutions exist when nonlinear aerodynamics is used. Although the high sideslip turning flight condition that corresponds to the second trim solution is unlikely in practice to be entered intentionally, it remains an interesting flight condition to study because it represents an unusual attitude situation that might be reached accidentally or in emergency conditions.

Figure 16 shows the damping of the first lag mode as a function of turn rate. When stall and compressibility effects are taken into account, this mode is unstable in straight descending flight and wide turns. The more simplified aerodynamic models still capture the loss of stability, and predict the mode to be neutrally stable. The stability levels increase with increasing turn rate. The mechanism identified in Ref. [6], namely the increase in aerodynamic damping in lag due to the increased aerodynamic loads developed by the rotor in the turn, explains the behavior of the results obtained with the linear and the nonlinear incompressible model. The additional increase in stability predicted when Mach number effects are also taken into account can be explained with the same argument used for the straight flight case, namely the effect of the nose-up pitching moments acting on the

blade. When angle of attack effects only are considered, the stability of the first lag mode in the high sideslip trim condition increases substantially. On the other hand, when the nonlinear compressible model was used, the quasilinearization algorithm failed to converge for all but one of the combinations of parameters used in this study to describe the high sideslip flight conditions. For the case in which convergence occurred all the modes were weakly stable, however it was impossible to identify the mode corresponding to each characteristic exponent. Because of these convergence difficulties, no results are shown in the figures for the high sideslip calculations using nonlinear compressible aerodynamics. The convergence difficulties also suggest that in this unusual flight condition severe aeroelastic instabilities may occur.

Moderately high turn rates in descending turns were observed to be destabilizing for the second lag mode in Ref. [6], with critical turn rates between 20 and 30 deg/sec. The loss of damping remains when stall and compressibility effects are included in the model, as shown in Figure 17 except that the critical turn rates are now reduced to about 10 deg/sec. The stability level increases with higher turn rates. This increase, however, is not captured if the Mach number effects are not modeled. In this case, the second lag mode is predicted to become unstable for a turn rate of about 15 deg/sec, with the instability increasing with increasing turn rate, and with the high sideslip condition being more unstable that the basic, or low sideslip, trim condition. The behavior of the first torsion mode appears from Figure 18 to be qualitatively similar to that in level turns. Thus the stability of this mode decreases for high turn rates, but the mode remains very well damped. The loss of stability is not captured by the linear incompressible aerodynamic model. Finally, the real parts of the characteristic exponents for the first three flap modes are grouped in Figure 19. The behavior of the three modes with increasing turn rate is qualitatively similar. They remain very well damped throughout the range of turn rates, with some loss of stability predicted at high turn rates. A severe destabilization occurs in the high sideslip trim condition, but even in this case no flap mode becomes unstable.

Assessment of problem nonlinearity

When linear incompressible aerodynamics is used, the nonlinearity of the aeroelastic stability and response problem is due to the kinematics of moderate elastic deflections. These kinematic nonlinearities are relatively weak. On the other hand, the modeling of stall and Mach number effects may introduce strong nonlinearities. Whether or not the aeroelastic problem as a whole becomes strongly nonlinear depends on the size and the strength of the stall, or near stall, regions over the rotor disk. An assessment of the nonlinearity of the aeroelastic problem is required to determine the reliability of linearized stability analyses, such as those based on Floquet theory.

A quantitative evaluation of the nonlinearity of the problem is a very complex task, not attempted in this study. However, a qualitative evaluation was carried out by observing the changes in the characteristic exponents, when the trim values of the collective pitch θ_0 were perturbed by $\Delta\theta_0 = \pm 5\%$. (The perturbed configurations were not retrimmed.) The stability of a linear system remains unchanged when the equilibrium position is changed. On the other hand, the linearized stability of a nonlinear system generally depends on the equilibrium position about which the linearization is carried out. Therefore, the size of the variations of the characteristic exponents due to the perturbations $\Delta\theta_0$ was taken as indicative of the overall nonlinearity of the aeroelastic problem.

Figures 20 and 21 show the real parts of the characteristic exponents of the first lag mode ζ_{L1} and of the first torsion mode ζ_{T1} respectively. Each figure contains the results obtained with the trim value of the collective pitch θ_0 and with the perturbed values $\theta_0 \pm \Delta\theta_0$, for both the linear incompressible and the nonlinear compressible aerodynamic models.

Figure 20 shows that the stability of the first lag mode changes by about 10% for 5% changes in collective pitch, for all the turn rates considered. The stability level increases for increasing θ_0. Introducing nonlinear aerodynamics increases the changes in ζ_{L1}, by amounts that vary rather widely in magnitude and sign depending on turn rate and sign of the collective pitch perturbation. The increased nonlinearity of the problem with refined aerodynamics is particularly evident in Figure 21. This figure shows that when linear aerodynamics is used, the stability of the first torsion mode remains essentially unaffected by $\Delta\theta$ for all the flight conditions considered. When nonlinear aerodynamics is used, the stability of the mode becomes increasingly sensitive to changes in θ_0 as the turn rate increases. For a turn rate of 16 deg/sec, the loss of stability for $\Delta\theta_0 = +5\%$ is almost of 40%. In both Figure 20 and 21 the largest differences, compared with the linear aerodynamics case, occur for perturbations $\Delta\theta_0 = +5\%$ that increase the size of the regions of the rotor disk at or near stall. Results not presented here show that, of the remaining modes, the second lag mode exhibits variations that are fairly similar to those of the first mode, and the first flap mode behaves similarly to the first torsion mode. The variations for the second and third flap mode are relatively small.

Figures 20 and 21 also suggest that particular care should be exercised in correlating the results of aeroelastic stability analyses and wind tunnel or flight tests, especially when stall or Mach number effects may be prevalent. In fact, the $\pm 5\%$ perturbations in collective pitch used in the figures correspond to actual variations of 0.6 degrees at most. Therefore it is possible that relatively large discrepancies between analytical and experimental results may result due to inaccuracies in defining test conditions, such as the rotor pitch control settings.

Conclusions

An aeroelastic stability and response analysis, which includes quasi-steady stall and compressibility effects on the lift, drag, and pitching moment characteristics of the airfoil, for hingeless rotor helicopters performing steady coordinated turns has been presented in this paper. Several limitations of previous analyses are removed. However, a number of assumptions made in the derivation of the mathematical model remain, and

are necessary in order to simplify the treatment of this very complex aeromechanical problem. The validity of these assumptions should be taken carefully into account in evaluating and extending the results of this study.

The results presented in this paper refer to soft-inplane hingeless rotor blades, and indicate the following trends:

1. The aeroelastic stability of the lag modes increases in a level turn. The damping of these modes increases with increasing turn rate. Neglecting Mach number effects on the airfoil characteristics may lead to underestimating the lag damping.

2. In descending flight conditions, the first lag mode is unstable in straight flight and wide turns, and is stabilized by increasing turn rates. The stability of the second lag mode decreases substantially in descending left turns, but the mode remains stable. The minimum damping, predicted to occur at turn rates of 20-25 deg/sec when using a linear aerodynamic model, moves to about 10 deg/sec when nonlinear compressible aerodynamics is used.

3. The first torsion mode and the first three flap modes experience a decrease in stability at high turn rates in both level and descending turns. This modes, however, are well damped, and remain stable despite the loss of damping.

4. One of the key factors in determining the aeroelastic behavior of the rotor blade is the presence of nose-up pitching moments over large portions of the rotor disk. These in turn are due to the specific shape of the $c_m(\alpha, M)$ curves of the airfoil, namely the nose-up pitching moments at angles of attack below stall. Therefore the conclusions of this study are limited to blades with airfoils that have this c_m behavior.

5. The increased nonlinearity of the problem, caused by the aerodynamic model, can manifest itself in multiple solutions to the coupled trim problem. The additional solution identified in this study corresponded to a high-sideslip flight configuration, with substantial degradation of the aeroelastic stability of the rotor.

6. The nonlinearity of the problem also causes the results to be very sensitive to changes in the equilibrium position about which the equations are linearized. Therefore great care has to be exercised in theory-experiment correlation exercises. In fact relatively large discrepancies may be erroneously attributed to inadequate theories or deficiencies in the test, when they may be actually due to inaccuracies in defining the test conditions.

Acknowledgements

This work was initiated with the support of the Army Research Office, Contract No.DAAL-03-88-C-002, technical monitors Dr. Robert Singleton and Dr. Tom Doligalski. The support of the Computer Science Center of the University of Maryland, where all the calculations were performed, is also acknowledged.

References

[1] Chopra, I., "Perspectives in Aeromechanical Stability of Helicopter Rotors," *Proceedings of the American Helicopter Society National Specialists' Meeting on Rotorcraft Dynamics*, Arlington, Texas, November 1989, to appear in *Vertica*.

[2] Friedmann, P., "Rotary-Wing Aeroelasticity with Application to VTOL Vehicles," Paper AIAA-90-1115-CP, *Proceedings of the AIAA/ASME /ASCE/AHS 31st Structures, Structural Dynamics and Materials Conference*, Long Beach, California, 2-4 April 1990, Part 3, pp. 1624-1670.

[3] Chen, R.T.N., and Jeske, J.A., "Kinematic Properties of the Helicopter in Coordinated Turns," NASA Technical Paper 1773, April 1981.

[4] Chen, R.T.N., and Jeske, J.A., "Influence of Sideslip on the Helicopter in Steady Coordinated Turns," *Journal of the American Helicopter Society*, Vol.27, No.4, pp. 84-92.

[5] Chen, R.T.N., "Flight Dynamics of Rotorcraft in Steep High-g Turns," *Journal of Aircraft*, Vol.21, No.1, January 1984, pp. 14-22.

[6] Celi, R., "Hingeless Rotor Dynamics in Coordinated Turns," Paper AIAA-90-1117-CP, *Proceedings of the AIAA/ASME/ASCE/AHS 31th Structures, Structural Dynamics and Materials Conference*, Long Beach, California, 2-4 April 1990, Part 3, pp. 1679-1689.

[7] Celi, R., and Friedmann, P., "Rotor Blade Aeroelasticity in Forward Flight with an Implicit Aerodynamic Formulation," *AIAA Journal*, Vol. 26, December 1988, pp. 1425-1433 .

[8] Celi, R., "Effect of Hingeless Rotor Aeroelasticity on Helicopter Trim and Longitudinal Stability Using Quasilinearization," Paper AIAA-88-4366-CP, *Proceedings of the 1988 AIAA Atmospheric Flight Mechanics Conference*, Minneapolis, Minnesota, August 1988.

[9] Shamie, J., and Friedmann, P., "Effect of Moderate Deflections on the Aeroelastic Stability of a Rotor Blade in Forward Flight," Paper No.24, *Proceedings of the Third European Rotorcraft Forum*, Aix-en-Provence, France, September 1977.

[10] Beddoes, T.S., "Representation of Airfoil Behaviour," *Vertica*, Vol. 7, No. 2, 1983, pp.183-197.

[11] Ormiston, R.A., and Bousman, W.G., "A Study of Stall-Induced Flap-Lag Instability of Hingeless Rotors," *Journal of the American Helicopter Society*, Vol.20, No.1, January 1975, pp. 20-30.

[12] Bramwell, A.R.S., *Helicopter Dynamics*, Edward Arnold, London, 1976, pp. 105-110.

[13] Johnson, W., *Helicopter Theory*, Princeton University Press, 1980, pp. 139-141.

[14] Wolkovitch, J., "Analytical Prediction of Vortex-Ring Boundaries for Helicopters in Steep Descents," *Journal of the American Helicopter Society*, Vol. 17, No. 3, July 1972, pp. 13-19.

[15] Peters, D.A., and Chen, S.Y., "Momentum Theory, Dynamic Inflow, and the Vortex-Ring State," *Journal of the American Helicopter Society*, Vol. 27, No. 3, July 1982, pp. 18-24.

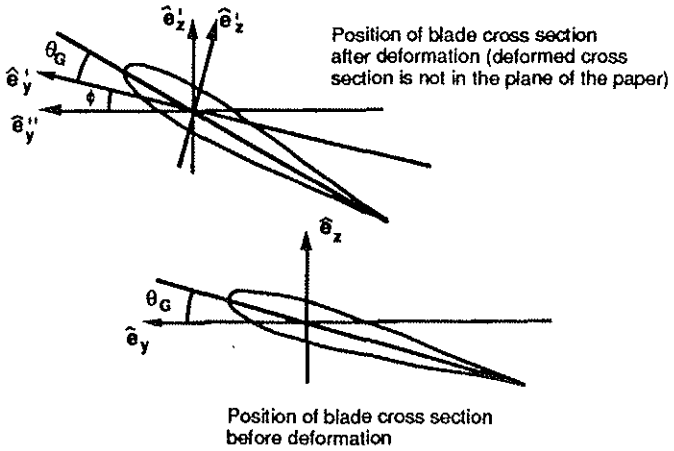

Figure 1: Deformed and undeformed blade coordinate systems (adapted from Ref.[9])

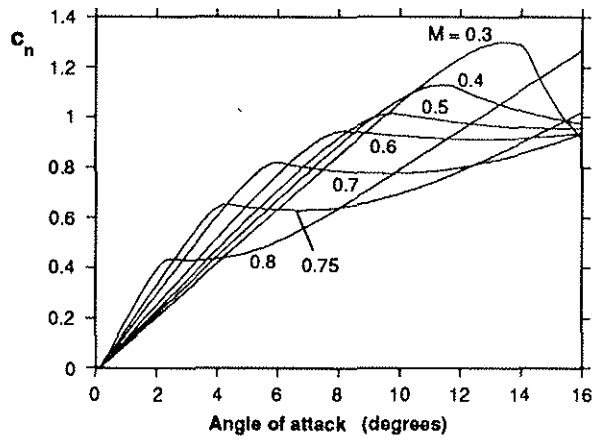

Figure 2: Airfoil normal force coefficient (adapted from Ref.[10]).

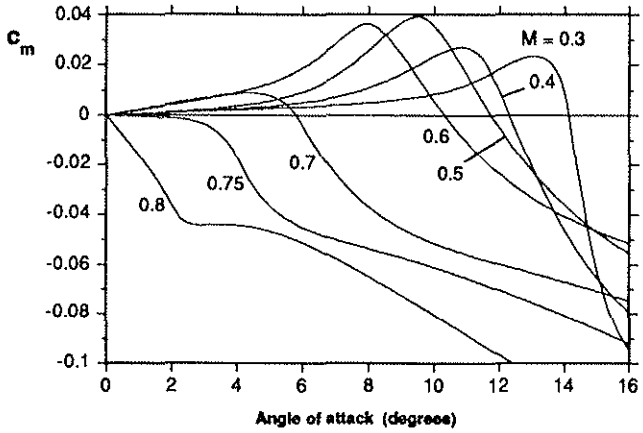

Figure 3: Airfoil pitching moment coefficient about quarter chord (adapted from Ref.[10]).

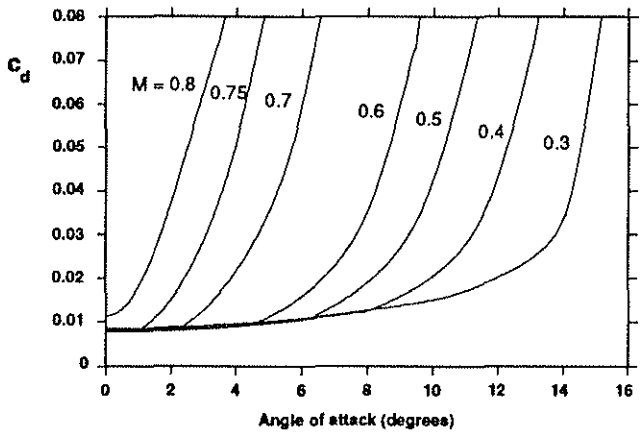

Figure 4: Airfoil drag coefficient (adapted from Ref.[10]).

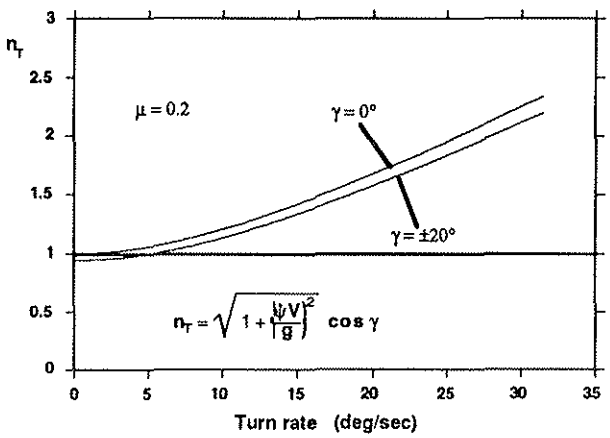

Figure 5: Load factor n_T in steady coordinated turns.

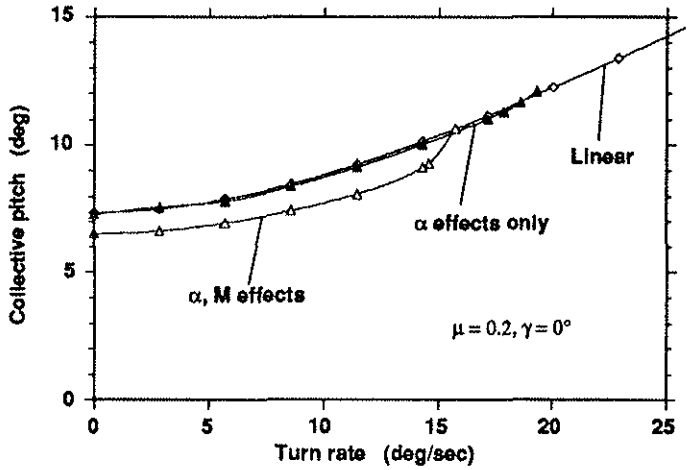

Figure 6: Effect of aerodynamic modeling assumptions on the collective pitch required for trim; level turn.

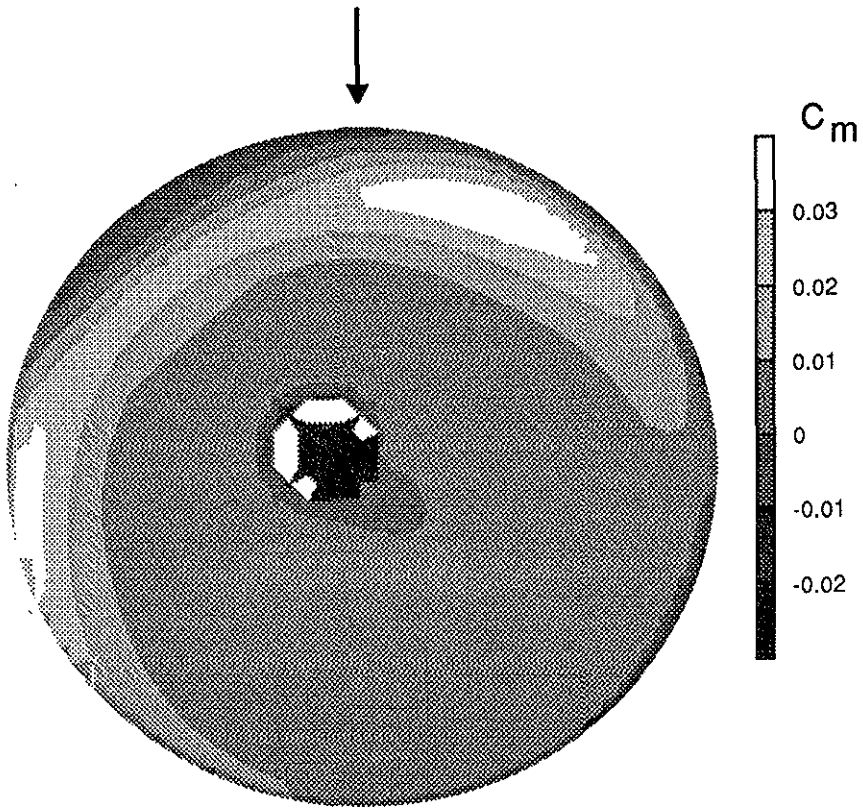

Figure 7: Distribution of pitching moment coefficient c_m ; $\mu = 0.2, \dot{\psi} = 0, \gamma = 0^o$.

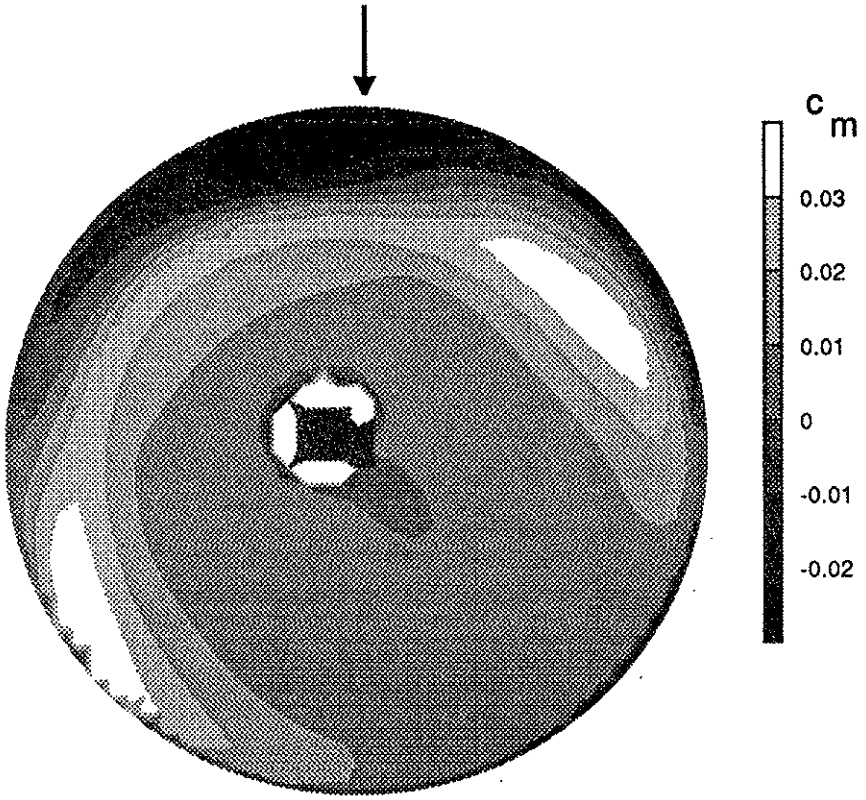

Figure 8: Distribution of pitching moment coefficient c_m; $\mu = 0.2, \dot{\psi} = 16$ deg/sec, $\gamma = 0°$.

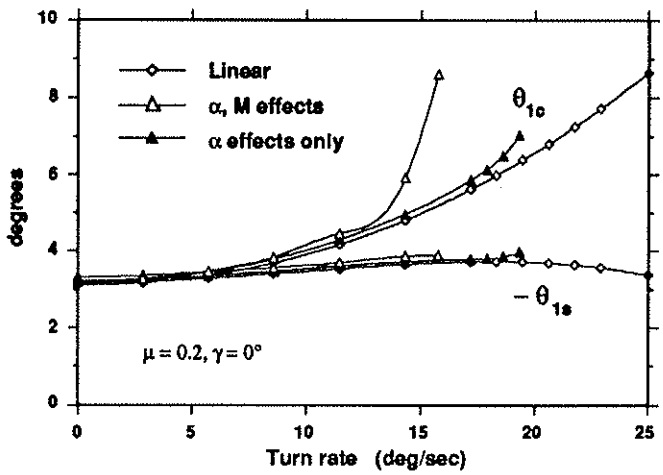

Figure 9: Effect of aerodynamic modeling assumptions on the longitudinal and lateral cyclic pitch required for trim; level turn.

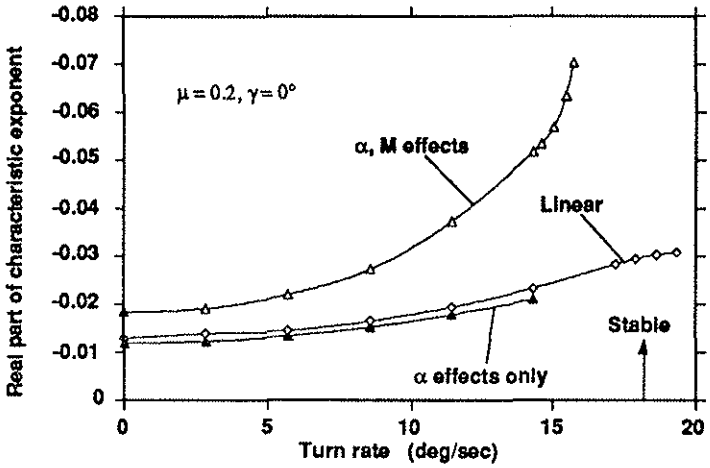

Figure 10: Effect of aerodynamic modeling assumptions on the stability of the first lag mode.

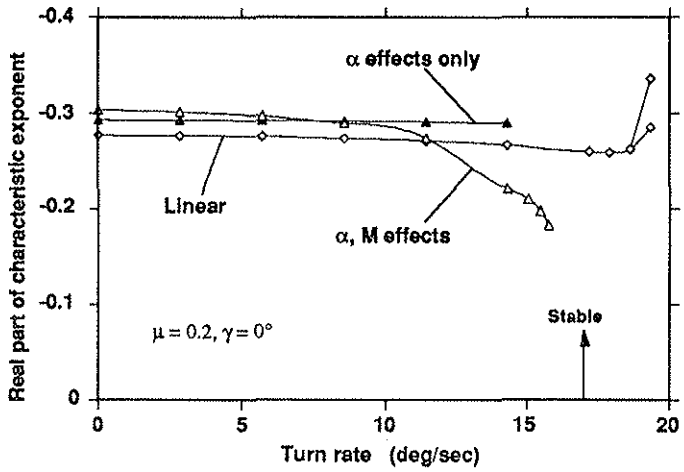

Figure 11: Effect of aerodynamic modeling assumptions on the stability of the first torsion mode.

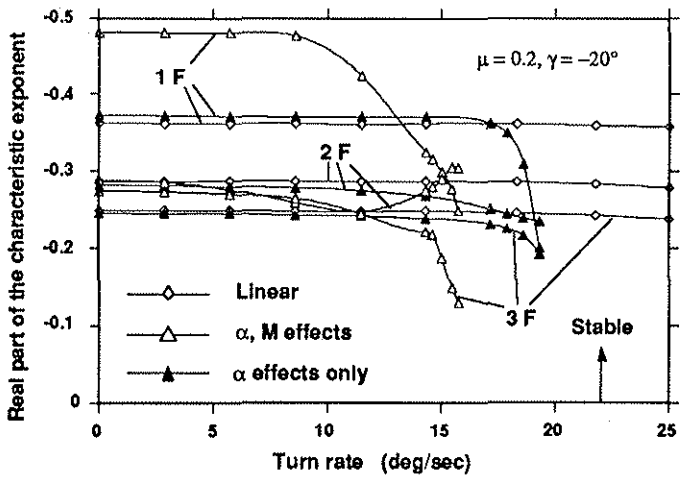

Figure 12: Effect of aerodynamic modeling assumptions on the stability of the lowest three flap modes.

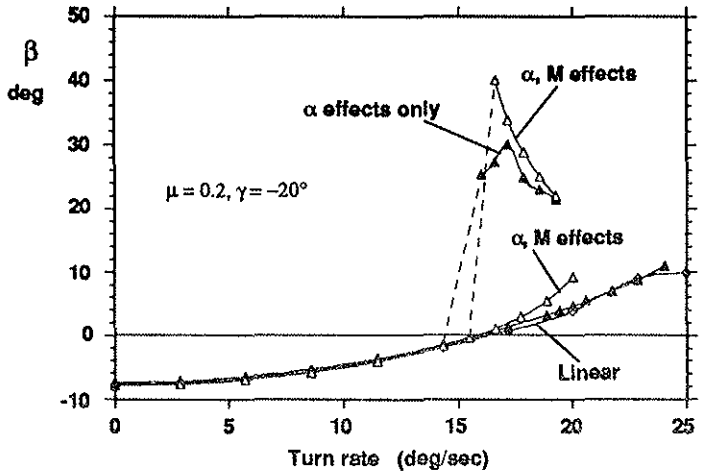

Figure 13: Sideslip angles in steady, coordinated, descending left turns.

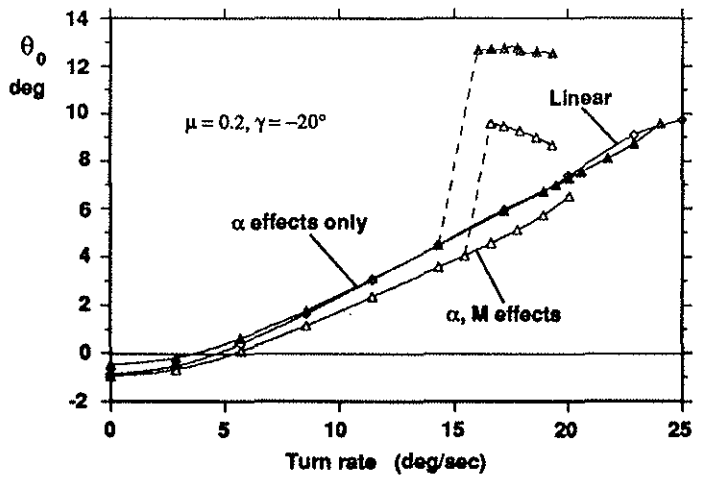

Figure 14: Collective pitch settings in steady, coordinated, descending left turns.

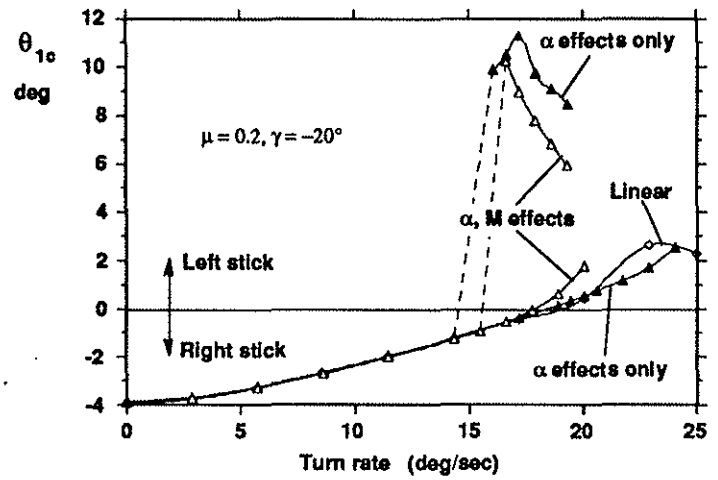

Figure 15: Lateral cyclic pitch settings in steady, coordinated, descending left turns.

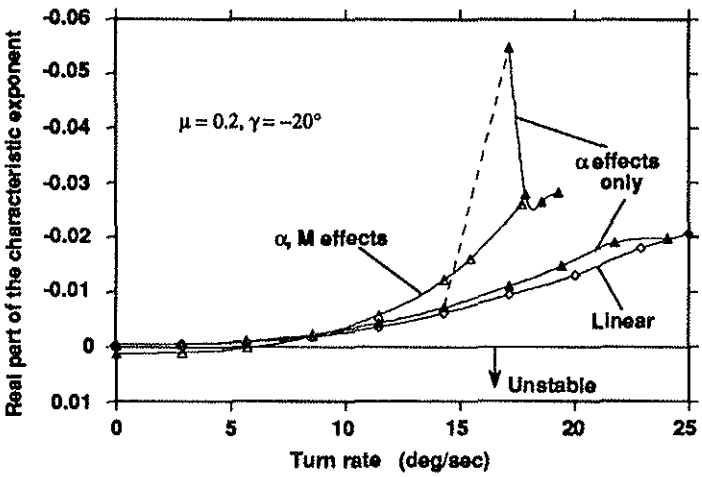

Figure 16: Effect of aerodynamic modeling assumptions on the stability of the first lag mode. (Data for high sideslip trim solution with nonlinear compressible aerodynamics not shown.)

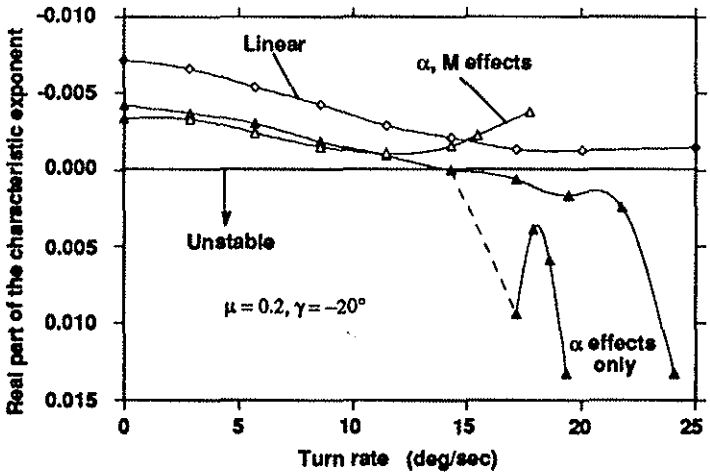

Figure 17: Effect of aerodynamic modeling assumptions on the stability of the second lag mode. (Data for high sideslip trim solution with nonlinear compressible aerodynamics not shown.)

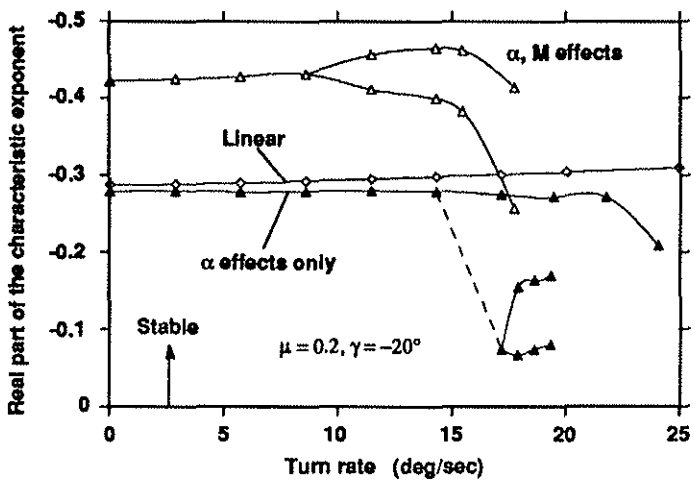

Figure 18: Effect of aerodynamic modeling assumptions on the stability of the first torsion mode. (Data for high sideslip trim solution with nonlinear compressible aerodynamics not shown.)

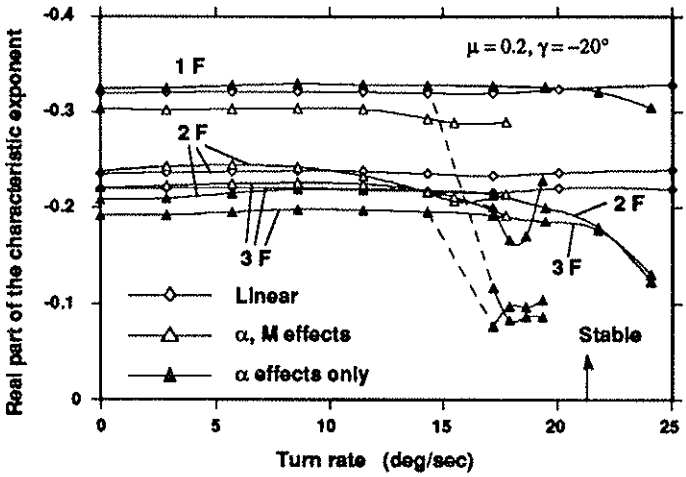

Figure 19: Effect of aerodynamic modeling assumptions on the stability of the three lowest flap modes. (Data for high sideslip trim solution with nonlinear compressible aerodynamics not shown.)

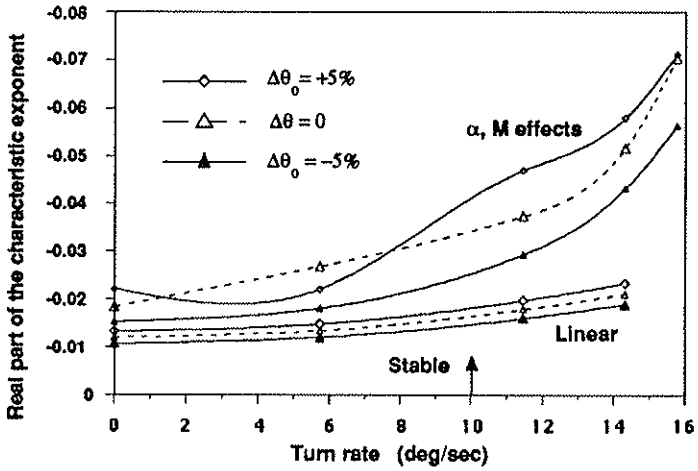

Figure 20: Changes in characteristic exponent of the first lag mode for a $\pm 5\%$ change in collective pitch θ_0; $\mu = 0.2, \gamma = 0°$.

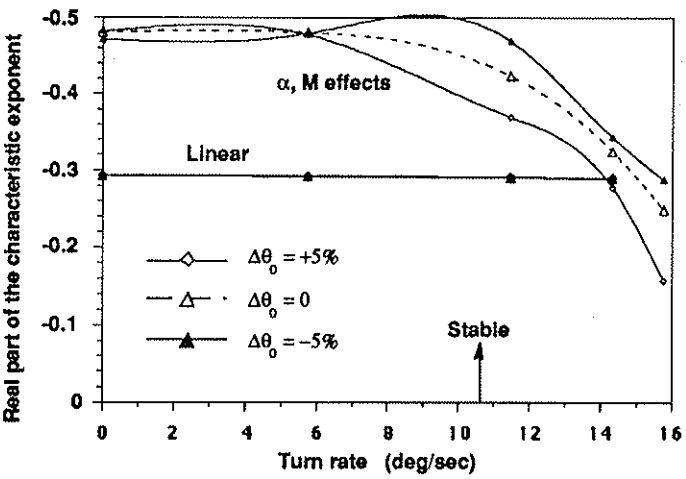

Figure 21: Changes in characteristic exponent of the first torsion mode for a $\pm 5\%$ change in collective pitch θ_0; $\mu = 0.2, \gamma = 0°$.